Indian Geotechnical Journal, 22 (3), 1992

On Modeling Stress-Strain and Dilatant Behaviour of Cohesionless Soil

by

Omar Faruque*

M. Musharraf Zaman**

A. Abdumrahee***

Introduction

Many constitutive models have been developed in the past for cohesionless soil using the framework of plasticity theory [Abduljauwad et al., 1989; Chang, 1985; Dafalias and Harrmann, 1982; De Boer, 1988; Desai, 1980; Desai and Faruque, 1984; Desai et al., 1986; DiMaggio and Sandler, 1971; Drucker et al., 1957; Faruque and Desai, 1985; Faruque and Chang, 1986; Faruque, 1987; Faruque and Zaman, 1989; Ghaboussi and Momen, 1982; Hirai, 1987; Lade and Duncan, 1975; Lade, 1977; Mroz et al., 1978; Pooroshasb and Pietruszezak, 1985; Prevost, 1978; Sandler, 1976; Valanis and Read, 1982; Zaman et al., 1982; Zienkiewicz et al., 1975]. A majority of these models emphasize the characterization of stress-strain response and do not adequately address the volumetric behavior. For cohesionless soil, characterization of volumetric response is of particular importance because such soil can undergo significant volume change during shearing.

Past experimental investigations on cohesionless soil have revealed two characteristic states in its stress-strain response during shearing (Fig. 1) [Abduljauwad et al., 1989; Chang, 1985; Desai and Faruque, 1984; Faruque and Zaman, 1989; Fukushima and Tatsuoka, 1984; Hardin, 1989; Lade and Duncan, 1975; Loung, 1984]. One of these characteristic states (e.g. point 1 in Figs. 1*a* and 1*b*) is attained as the soil approaches the state of failure. In this state the soil experiences progressive shear deformation under constant volume (i.e. zero rate of volumetric strain). The second characteristic state (e.g., point 2 in Figs. 1*a* and 1*b*) is attained when the rate of volumetric strain momentarily vanishes as the soil passes from the compressive mode of deformation to the dilatant mode of deformation during shearing. For a given cohesionless soil, these characteristic states generally depend upon the initial relative density of the soil as well as the confining pressure at which

* Former Visiting Assistant Professor
** Associate Professor
*** Graduate Research Assistant

School of Civil Engineering and Environmental Science University of Oklahoma, Norman, OK 73019

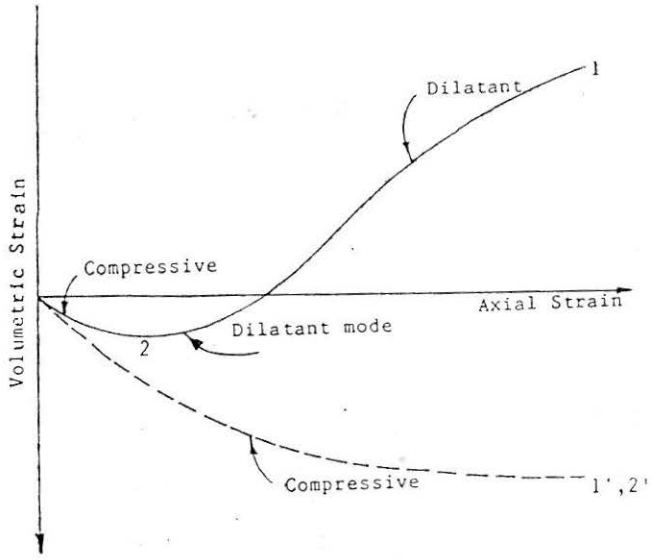

FIGURE 1(a) Typical Volumetric-Axial Strain Response of Cohesionless Soil

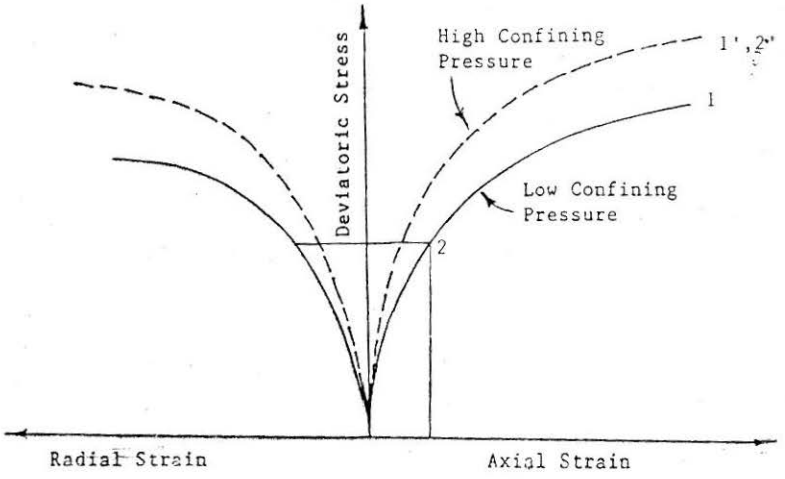

FIGURE 1(b) Typical Stress-Strain Response of Cohesionless Soil

the test is performed [Abduljauwad, 1989; Fukushima and Tatsuoka, 1984; Hardin, 1989; Lade, 1977; Loung, 1980; Pooroshasb and Pietruszezak, 1985]. When shearing occurs under a moderately high confining pressure, cohesionless soils often exhibit compressive volumetric response up to failure indicating merging of the two characteristic states (e.g., points 1′ and 2′ in Figs. 1*a* and 1*b*). This may also be true when a relatively loose soil undergoes shearing under moderately high confining pressure. With the exception of the above cases, the two characteristic states for a given cohesionless soil are distinct.

The concepts of characteristic states and their representation as characteristic state surfaces in the stress space are introduced in this paper to describe volumetric behavior of cohesionless soil during shearing. Explicit forms of the characteristic state surfaces in the stress space are proposed and used to develop a constitutive model based on the framework of plasticity theory. The general forms of the characteristic state surfaces proposed are verified using drained shear test data for a fine sand. Stress-strain and volumetric-axial strain responses are predicted using the proposed model and good correlations are observed with experimental data.

Short Coming of Some of the Existing Models

There are some shortcomings in the existing plasticity based models for cohesionless soil in regard to characterization of dilatancy. For illustration, consider the elements of a cap type constitutive model as shown in Fig. 2 [Abduljauwad et al., 1989; Desai and Faruque, 1984; Desai et al., 1986; DiMaggio and Sandler, 1971; Drucker et al., 1957; Faruque and Desai, 1985; Faruque and Chang, 1986; Faruque, 1987; Lade and Duncan, 1975; Lade, 1977; Mroz et al., 1978; Pooroshasb and Pietruszeazak, 1985]. The yield cap originates from J_1 axis and terminates at the failure envelope where the tangent to the yield cap is horizontal. As a result, within the framework of associated plasticity theory, only compressive volumetric strain will be obtained for stress space lying on the yield cap including point L (Fig. 2). Since the normal to the yield cap is vertical at point L, it represents the onset of dilatancy that corresponds to point 2 (i.e. the second characteristic state) in Fig. 1a. However, point L also lies on the failure envelope that corresponds to point 1 (i.e. the first chracteristic state) in Fig. 1a. This representation is inconsistent because points 1 and 2 are distinctly different for cohesionless soil under general conditions as evident from Fig. 1a. An exception of this is possible when a cohesionless soil is subjected to high confining pressures where the two characteristic states merge as shown by points $1'$ and $2'$ in Fig. 1a.

In consistencies also exist in models which claim to characterize the onset of dilatancy and subsequent volumetric response of cohesionless soil [Desai and Faruque, 1984; Fukushima and Tatsuoka, 1984; Ghaboussi and Momen, 1982; Zienkiewicz et al., 1975]. This can be illustrated with the help of Fig. 3. It is evident that the line representing the onset of dilatancy deviates increasingly from the failure envelope with increasing confining pressure. This contradicts experimental observation which reveals that the line representing the onset of dilatancy approaches the failure envelope with increasing confining pressure. The primary reason for such flaws in these constitutive models is the selection of yield and/or plastic potential functions on an adhoc basis without any consideration for the second characteristic state. Thus, the line representing the onset of dilatancy in these

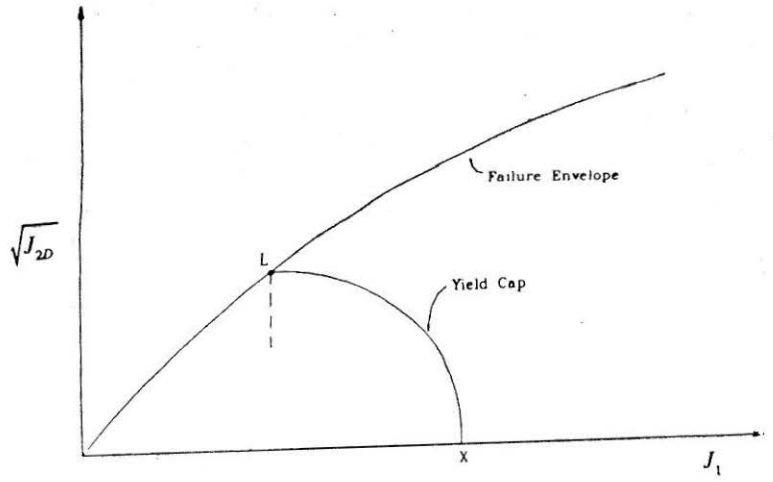

FIGURE 2 Elements of a Typical Cap Type Constitutive Model

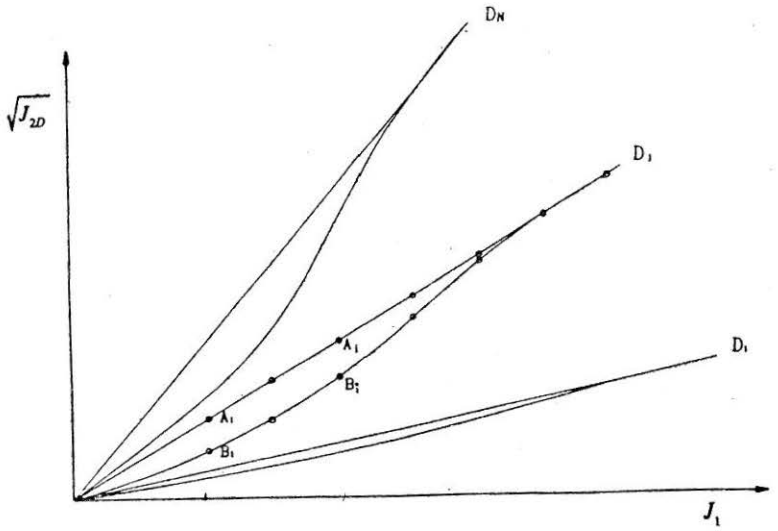

FIGURE 3 Schematic Representation of the Two Characteristic State Lines for Various Initial Relative Densities

models is essentially a characteristic of the selected functions (i.e., yield and/or plastic potential) and not the second characteristic state that is unique to a cohesionless soil.

FORMULATION OF THE PROPOSED MODEL

Characteristic State Surfaces

The characteristic states of a cohesionless soil can be represented in the form of characteristic state surfaces in the J_1—$\sqrt{J_{2D}}$—D space as shown

schematically in Figs. 4a and 4b. The variables J_1 and $\sqrt{J_{2D}}$ denote the first invariant of the stress tensor and the second invariant of the deviatoric stress tensor, respectively. For a given initial relative density, the characteristic state surfaces degenerate to the characteristic state lines in the J_1—$\sqrt{J_{2D}}$ space. For various values of initial relative density, D_i (i=1,..., N), the characteristic state lines are shown schematically in Fig. 3. It is evident that the two characteristic state lines are distinct in most parts and tend to merge as the confining pressure becomes high. Also, the deviation of the characteristic state lines increases with the increase in initial relative density. For a given initial relative density, the characteristic state surfaces can be viewed as characterististic state lines on the J_1—$\sqrt{J_{2D}}$ plane.

First Characteristic State Line

Experimental observations have shown that the first characteristic state line (CSL-1) for cohesionless soil is an approximate straight line on the

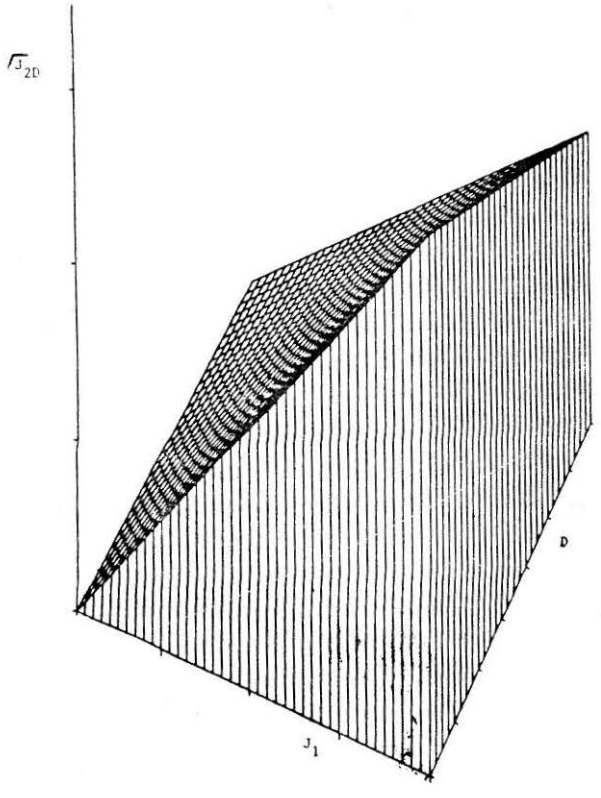

FIGURE 4a. Schematic Representation of the First Characteristic State Surface in J_1—$\sqrt{J_{2D}}$—D Space

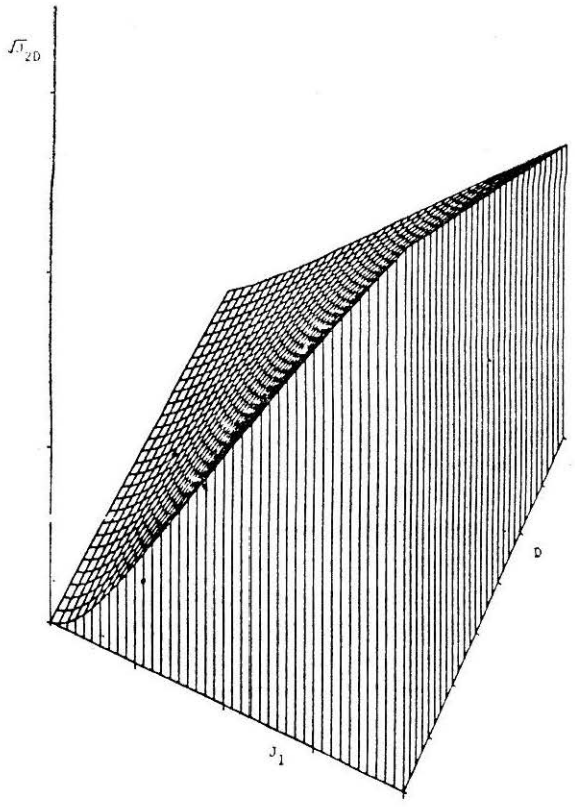

FIGURE 4b. Schematic Representation of the Second Characteristic State Surface in J_1—$\sqrt{J_{2D}}$—D Space

J_1—$\sqrt{J_{2D}}$ plane. This shows that the shear strength of such soil increases linearly with the confining pressure which is consistent with the Mohr-Coulomb theory of failure of granular soils. The slope of the characteristic state line (CSL-1) is a measure of the internal frictional coefficient and increases with increasing initial relative density, D, due to increasing compactness of the grains. Fig. 5 shows the plot of a representative CSL-1 for a typical cohesionless soil at a given initial relative densiy.

For a given initial relative density, the first characteristic state line for cohesionless soil also depends upon the orientation, θ, of a stress path on the octahedral plane. A common definition of θ is given by

$$\theta = \tfrac{1}{3} \cos^{-1} \left[\frac{3\sqrt{3}\ J_{3D}}{2(J_{2D})^{3/2}} \right] \qquad (1)$$

where $J_{3D} = \frac{1}{3} S_{ij}S_{jk}S_{ki}$ is the third invariant of the deviatoric stress tensor, S_{ij}. The orientation θ lies in the range $0° \leqslant \theta \leqslant 60°$ where $\theta = 0°$ represents

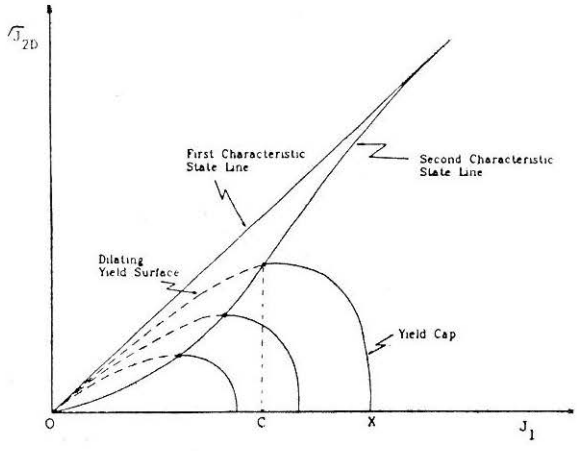

FIGURE 5 Schematic Representation of Yield Cap and Dilating Yield Surface on J_1—$\sqrt{J_{2D}}$ Space

a compression stress path and $\theta = 60°$ represents an extension stress path. As evident from experimental observations [Abduljauwad et al., 1989; Desai and Faruque, 1984; Faruque, 1987; Honamandebrahimi and Zaman, 1987], the slope of the first characteristic state line is maximum for $\theta = 0°$ and minimum for $\theta = 60°$.

In view of the above discussion, the equation of the first characteristic state line (CSL-1) can be written in the form

$$\sqrt{J_{2D}} = Mg(\theta)\, J_1 \tag{2}$$

where M is a material response function of the initial relative density, D, and $g(\theta)$ is a function that accounts for the change in the slope of CSL-1 with θ. Following the works of Podgorski [1985] and Faruque and Chang [1986], $g(\theta)$ can be expressed as

$$g(\theta) = [Cos\{\tfrac{1}{3}\, Cos^{-1}\,(-A'\, Cos3\theta)\}]^{-1} \tag{3}$$

where A′ is assumed to be unity to satisfy convexity of the failure surface on the octahedral plane. Assuming M_o as the value of $M(D)$ at D=0 (i.e. loosest possible state), a functional form of $M(D)$ can be written as

$$M(D) = M_0\,[1 + h_1(D)] \tag{4}$$

in which $h_1(D)$ is a response function that determines the ratio $M(D)/M_o$ for a given initial relative density, D, and satisfies the condition $h_1(0) = 0$. Note that $h_1(D)$ is a monotonically increasing function of D and attains maximum value at $D = 1$ (i.e., the densest possible state). Denoting the maximum value of $h_1(D)$ as λ_1, the following form of $h_1(D)$ is proposed

$$h_1(D) = \lambda_1\, D^{\eta_1} \tag{5}$$

where the exponent η_1 signifies the shape of the function $h_1(D)$. In general, $h_1(D)$ can assume the representations shown by curves A, B and C in Fig. 6.

The rate of change of $M(D)$ with D (i.e., dM/dD) generally decreases with increasing initial relative density. Therefore, curve A (Fig. 6) is an unlikely representation of $h_1(D)$. The proposed form of $h_1(D)$ in Eq. (5) can be validated using appropriate experimental data.

Second Characteristic State Line

Unlike the first characteristic state line (CSL-1), experimental observations as to the second characteristic state line is non-existent in the literature. It is, however, known that the second characteristic state tends to merge with the first characteristic state as the confining pressure becomes very high. As a result, the second characteristic state line should approach the first characteristic state line as the confining pressure increases. The proposed forms of CSL-2 on the J_1—$\sqrt{J_{2D}}$ plane for various initial relative densities are schematically shown in Fig. 3. For relatively lose cohesionless soils, the characteristic state lines are quite close as indicated in Fig. 3. For higher initial relative density, the deviation of the characteristic state lines increases. Referring to Fig. 3, an equation of the second characteristic state line (CSL-2) is proposed in the form

$$\sqrt{J_{2D}} = M(D)\,[1-N(D)\exp(-\mu\ \frac{J_1}{P_a})]\ g(\theta)\ J_1 \qquad (6)$$

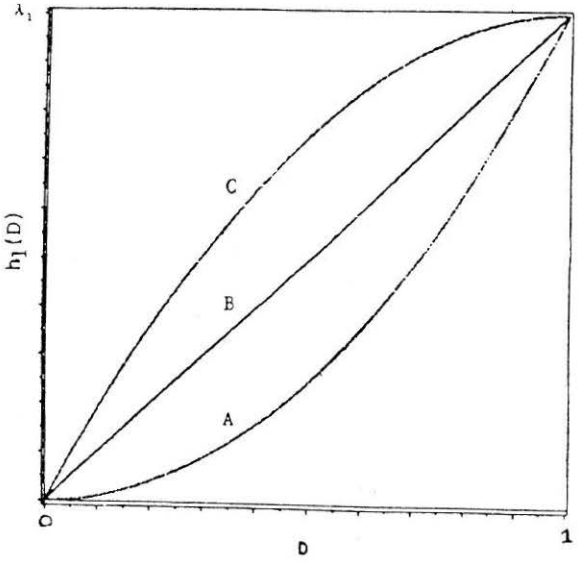

FIGURE 6 Schematic Representation of Function h_1 (D)

where μ is a material constant, P_a is the atmospheric pressure expressed in the same units as J_1 and N is a material response function of the initial relative density, D. For high values of J_1, the exponential term in Eq. (6) becomes negligible and thereby, Eq. (6) approaches the first characteristic state line defined by Eq. (1). Referring to Eq. (6), the secant slope $(\sqrt{J_{2D}}/J_1)$ at $J_1 = \theta$ is obtained as $M(D)$ $[1—N(D)]$ $g(\theta)$. Therefore, the material response function N determines the initial slope of the second characteristic state line at $J_1 = 0$. When $N(D) = 0$, both characteristic state lines have the same initial slope of M. Preliminary results on a beach sand [Faruque and Zaman, 1989] indicates that the initial slope of the second characteristic state line is smaller than $M(D)$ and in general, a function of the initial relative density, D. Assuming $N(D) = N_o$ at $D = 0$ (i.e., the loosest possible state), a functional form of $N(D)$ can be wrtten as

$$N(D) = N_0 [1 + h_2(D)] \tag{7}$$

where $h_2(D)$ determines the ratio $N(D) / N_o$ for a given D and satisfies the condition $h_2(D) = 0$. Following the analogy of $h_1(D)$, it is postulated that $h_2(D)$ is a monotonically increasing function of D and attains a maximum value of λ_2 at $D = 1$ (i.e., the densest possible state). In view of this the following form of $h_2(D)$ is proposed

$$h_2(D) = \lambda_2 D^{\eta_2} \tag{8}$$

The exponent η_2 in Eq. (8) dictates the shape of the function $h_2(D)$. The proposed form of $h_2(D)$ in Eq. (8) can be validated by using appropriate experimental data.

Compressive Yield Surface

Consistent with the definition of CSL-2, all states of stress below the second characteristic state line yield compressive volumetric strain only. Therefore, within the associated theory of plasticity, an yield surface between the J_1-axis and the second characteristic state line should be defined such that the normal to the yield surface at any point has non-negative slopes. Besides, the normal to the yield surface at the point of intersection with the second characteristic line (CSL-2) should be parallel to the $\sqrt{J_{2D}}$-axis. This is because, by definition, CSL-2 contains all stress states where the rate of volumetric deformation momentarily vanishes as the soil passes from the compressive mode of deformation to the dilatant mode of deformation during shearing. An elliptical yield surface that satisfies the above requirements is used in the proposed model and is shown schematically in Fig. 5. It is evident that the tangent to the yield surface at the intersection with J_1-axis is vertical. This ensures purely spherical response under hydrostatic loading and is required for an initially isotropic material. An equation of the compressive yield surface is proposed as

$$F_c = \sqrt{J_{2D}} - \sqrt{a^2 - 1/R^2(J_1 - C)^2}\, g(\theta) = 0 \tag{9}$$

where R is a constant associated with the ratio of the axes of the ellipse and is a material constant and, in general, C is a response function that denotes the value of J_1 at the point of intersection of the yield surface and the second characteristic state line. In Eq. (9), a represents the axis of the elliptical yield surface parallel to $\sqrt{J_{2D}}$ axis and is defined in terms of C as

$$a = M[1 - N \exp(-\mu C/P_a)]\, g(\theta) C \tag{10}$$

Note that elliptical yield surface has been used in other models such as cap model [Abduljauwad et al., 1989; Desai and Faruque, 1984; Desai et al., 1986; DiMaggio and Sandler, 1971; Drucker et al., 1957; Faruque and Desai, 1985; Faruque and Chang, 1986; Faruque, 1987; Lade and Duncan, 1975; Lade, 1977; Mroz et al., 1978; Pooroshasb and Pietruszezak, 1985] in the past and found to be satisfactory for the prediction of response in the compressive mode of deformation. However, other convex mathematical functions that satisfy the requirements of a yield surface discussed earlier may also be used.

The proposed model utilizes a nonassociated formulation to describe the volumetric response in the compressive regime. A plastic potential function, Q_c, is defined in the form

$$Q_c = \sqrt{J_{2D}} - \bar{A} \sqrt{a^2 - 1/R^2 (J_1 - C)^2}\, g(\theta) \tag{11}$$

where $\bar{A}$ is a material constant. Taking the derivatives of F_c and Q_c with respect to J_1, the following relationship can be obtained

$$\frac{\partial Q_c}{\partial J_1} = \bar{A} \frac{\partial F_c}{\partial J_1} \tag{12}$$

As evident from Eq. (12), the constant $\bar{A}$ signifies deviation from normality and should have a positive value. The condition $\bar{A} > 0$ is necessary to maintain compressive volumetric strain for stress states below CSL-2. For $\bar{A} = 1$, $Q_c = F_c$, which represents associated formulation.

Dilating Yield Surface

By definition, a dilating yield surface refers to the stress state's that causes dilating response at a material point. As described earlier, at a high confining pressure, cohesionless soil experiences compressive mode of deformation at all stages of loading up to failure. This indicates that the dilating yield surface is bounded by CSL-1 and CSL-2 at all times and identifies itself with the first characteristic state line (CSL-1) when the confining pressure is very high (Fig. 7). An equation of the dilating yield surface that satisfies the above requirements is proposed in the form

$$F_d = \sqrt{J_{2D}} - a\,[1 - (1 - J_1/C)^{MC/a}]\, g(\theta) \tag{13}$$

A schematic representation of Eq. (13) is shown in Fig. 5. As evident, the tangent to the dilating yield surface at the point of intersection with the second characteristic state line is horizontal and thereby satisfies slope compatibility with the compressive yield surface, $F_c = 0$. At $J_1 = 0$, the slope of the dilating yield surface is M and therefore, tangential to the first characteristic state line at that point.

It is evident from Fig. 5 that the normal to the dilating yield surface at any point has a non-positive slope and decreases with the stress state approching the first characteristic state line. As a result, within the associated theory of plasticity, the rate of dilatancy predicted by the model increases continuously as the stress paths approach the first characteristic state line. This is contrary to the definition of CSL-1 that contains all stress states for which a soil experiences progressive shear deformation at constant volume (i.e., zero rate of dilatancy). It is, therefore, necessary to incorporate some mechanism in the model that will enable it to predict zero rate of dilatancy when the stress state is on the characteristic state lines (both CSL-1 and CSL-2) and nonzero rate of dilatancy when the state of stress lies in between the characteristic state lines. In the proposed model, this is achieved by using non-associated formulation. To this end, a dilating potential function, Q_d, is defined by the following equations.

$$\frac{\partial Q_d}{\partial J_1} = q(J_1, J_{2D}) \quad \frac{\partial F_d}{\partial J_1} \tag{14}$$

$$\frac{\partial Q_d}{\partial J_{2D}} = \frac{\partial F_d}{\partial J_{2D}} \tag{15}$$

$$\frac{\partial Q_d}{\partial \theta} = \frac{\partial F_d}{\partial \theta} \tag{16}$$

where

$$q(J_1, J_{2D}) = \alpha \frac{(\beta+\gamma)^{\beta+\gamma}}{\beta^{\beta}\,\gamma^{\gamma}} (1-G)^{\beta} G^{\gamma} \tag{17}$$

in which

$$G(J_1, J_{2D}) = \frac{MJ_1 - \sqrt{J_{2D}}/g(\theta)}{MN \exp(-\mu J_1/P_a) J_1} \tag{18}$$

In above equations α, β and γ are material constants and the function $G(J_1, J_{2D})$ assumes a value of unity at CSL-2 and zero at CSL-1. Consequently, the function $q(J_1, J_{2D})$ becomes zero at the boundaries (CSL-2 and CSL-1) and is non-negative elsewhere. $q(J_1, J_{2D})$ has a maximum value of α at $G(J_1, J_{2D}) = \beta/(\beta+\gamma)$. Note that only derivatives of the potential function Q_d is required to obtain the elasto-plastic constitutive matrix. As an explicit form of Q_d is not necessary.

Hardening Behavior

In this work, modeling of soil response under monotonic loading is attempted using the concept of isotropic hardening plasticity. Both the compressive yield surface, F_c, and the dilating yield surface, F_d, are allowed to expand in the stress space to account for hardening during elasto-plastic deformation. The history of inelastic volumetric strain is frequently used to describe hardening of cohesionless soil during hydrostatic loading as well as shear loadings [DiMaggio and Sandler, 1971]. Commonly a hardening function is prescribed in terms of the accumulated plastic volumetric strain and the associated material constants are determined using hydrostatic compression test data only. It is important to realize that the mechanism of inelastic volume change during hydrostatic compression is quite different from that in shear. As a result, a hardening function, with its constants determined from hydrostatic compression test data, generally cannot describe elasto-plastic stress-strain and volumetric behaviour during shearing in a rational manner. This problem can be resolved by expressing a hardening function in terms of two parameters, ξ and r_d which are defined in terms of the incremental plastic strain tensor $d\varepsilon_{ij}^p$ and the incremental deviatoric plastic strain tensor de_{ij}^p as follows

$$\xi = \int (d\varepsilon_{ij}^p \, d\varepsilon_{ij}^p)^{1/2} \tag{19}$$

$$r_d = \xi_d / \xi \tag{20}$$

where

$$\xi_d = \int (de_{ij}^p \, de_{ij}^p)^{1/2} \tag{21}$$

In the above equations, the symbol $\int$ denotes the history. Note that ξ_d and r_d have zero value throughout hydrostatic compression.

Referring to Fig. 5, the compressive yield surface, F_c, originates from the J_1 -axis (i.e. point X) and terminates at a point on the second characteristic state line (CSL-2) where J_1 assumes a value of C. The dilating yield surface, F_d, on the other hand, starts from the origin O and terminatss at CSL-2 where $J_1 = C$.

Since $X = (C + Ra)$, where R is the ratio of major to minor axis of the elliptical cap (Fig. 5) and a is the ordinate corresponding to $J_1 = C$, expansion of both F_c and F_d can be described conveniently by making X a (hardening) function of the parameters ξ and r_d as

$$X = \beta_1 \, \xi^{\eta} \tag{22}$$

where

$$\eta = \eta_1 \, [1 + \beta_2 \, r_d^{\eta_2}] \tag{23}$$

In Eqs. (22) and (23), β_1, β_2, η_1 and η_2 are material constants. An initially isotropic material, when subjected to a hydrostaitc state loading, experiences a spherical deformation only (i.e., $r_d = 0$ and $\xi = \xi_v$, where $\xi_v = \int 1/\sqrt{3 d\varepsilon_v^p} = 1/\sqrt{3}\ \varepsilon_v^p$, ε_v^p being the total volumetric plastic strain). The hardening function for this case reduce to

$$X = \beta_1\ \xi_v^{\eta_1} \tag{24}$$

The constants β_1 and η_1 can be evaluated by fitting Eq. (24) through X vs. ε_v^p plot of data points obtained from a hydrostatic compression test. Direct evaluation of β_2 and η_2 from experimental data is rather difficult. These constants are evaluated from experimental data by using a nonlinear optimization procedure.

ELASTO-PLASTIC CONSTITUTIVE RELATIONS

Using the concept of non-associative plasticity theory, incremental plastic strain tensor, $d\varepsilon_{ij}^p$, can be expressed as

$$d\varepsilon_{ij}^p = d\lambda\ \frac{\partial Q}{\partial \sigma_{ij}} \tag{25}$$

where Q is the plastic potential function and $d\lambda$ is an unknown scalar to be determined from the consistency condition of Prager, $dF = 0$, F being the yield function. Following the standard steps of the theory of plasticity, the elasto-plastic constitutive relation tensor, C_{ijkl}^{ep} can be written as

$$C_{ijkl}^{ep} = C_{ijkl}^{e} - \frac{C_{ijuv}^{e}\ \dfrac{\partial F}{\partial \sigma_{uv}}\ \dfrac{\partial Q}{\partial \sigma_{mn}}\ C_{mnkl}^{e}}{\dfrac{\partial F}{\partial \sigma_{pq}}\ C_{pqrs}^{e}\ \dfrac{\partial Q}{\partial \sigma_{rs}} - A(\xi, r_d, \sigma_{rs})} \tag{26}$$

where C_{ijkl}^{e} is the elastic constitutive tensor and $A(\xi, r_d, \sigma_{ij})$ is a measure of plastic modulus involving derivatives of the yield function F with respect to ξ and ξ_d and derivative of the potential function Q with respect to σ_{ij}. Equation (26) is valid in the compressive as well as the dilative regimes of shear deformation provided Q is appropriately defined. In the compressive regime, $Q = Q_c$ (Eq. 11), while in the dilative regime, $Q = Q_d$ defined implicitly by Eqs. 14-18.

Application

Drained shear test data [Abduljauwad et al., 1989] for a fine sand with an uniformity coefficient of 1.84 is used in this study to investigate the characteristic states and to verify the proposed constitutive model. A stress controlled cylindrical triaxial device is used. The density of the test samples

is in the range of 103.7 pcf to 105.6 pcf with an average relative density, D, of 81%. The characteristic state lines (CSL-1 and CSL-2) obtained from the experimental data are depicted in Fig. 7. It is evident that the observed characteristic state lines are in agreement with the general forms proposed in the model. The second characteristic state line shows substantial deviation from CSL-1 in the low confining pressure range and tends to approach CSL-1 as the confining pressure becomes high.

Prediction of stress-strain response requires evaluation of material constants associated with the model. Since the tests were performed at a constant relative density ($D = 81\%$), only the following set of parameters were evaluated using a nonlinear optimization technique: $R = 6.134$, $\beta_2 = 0.828$, $\eta_2 = 3.37$, $\bar{D} = 0.7275$, $\mu = 0.06$, $N = 0.442$, $\alpha = 0.318$, $\beta = 0.57$ and $\gamma = 0.599$. The values of K and G are determined from experimental data as $K = 27369 + 407.7 * P$ and $G = 9598 + 317.6 * P$ where P is the confining pressure in *KPa*. The constants $\beta_1 = 1.61 * 10^6$ and $\eta_1 = 1.17$ are evaluated from the hydrostatic compression test data.

Fig. 8*a* shows a comparison of the stress-strain response of a *CTC* (Conventional Triaxial Compression) test performed at a confining pressure of 207 *Kpa* (30 psi). Evidently the model prediction is in excellent agreement with the experimental observation for the entire range of loading. A similar comparison of volumetric-axial strain response is shown in Fig. 8*b*. The onset of dilatancy as well as the volumetric response in the dilative regime are predicted very well by the model.

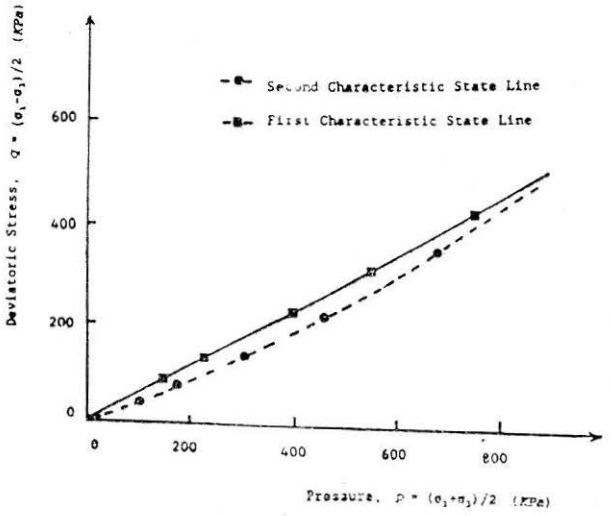

FIGURE 7 The Two Characteristics State Lines for a Beach Sand Obtained from Experimental Data at 81% Initial Relative Density

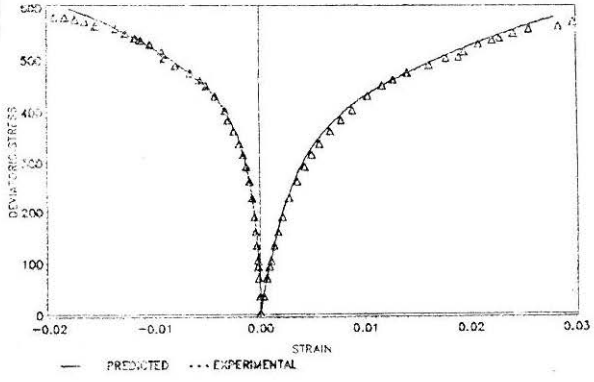

FIGURE 8a Comparison of Stress-Strain Response for Conventional Triaxial Compression Test at 30 psi Confining Pressure

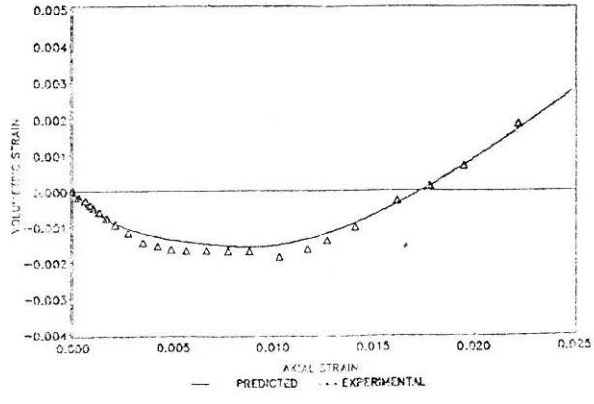

FIGURE 8b Comparison of Volumetric-Axial Strain Response for Conventional Triaxial Compression Test at 30 psi Confining Pressure

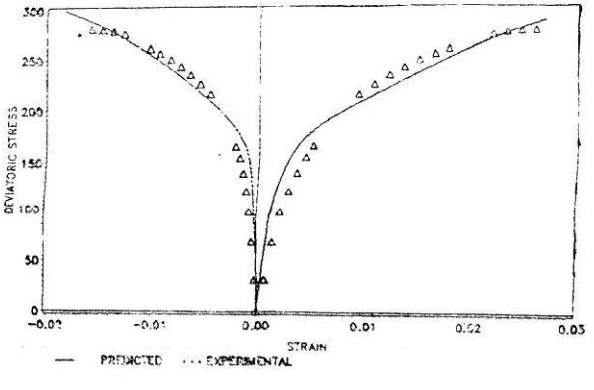

FIGURE 9a Comparison of Stress-Strain Response for Conventional Triaxial Compression Test at 15 psi Confining Pressure

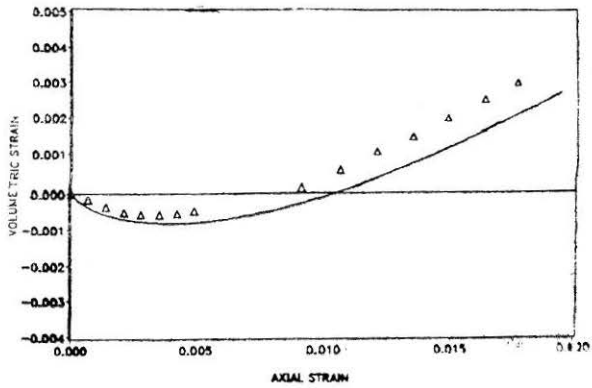

FIGURE 9b Comprearison of Volumetric-Axial Strain Response for Conventional Compression Test at 30 psi Confining Pressure

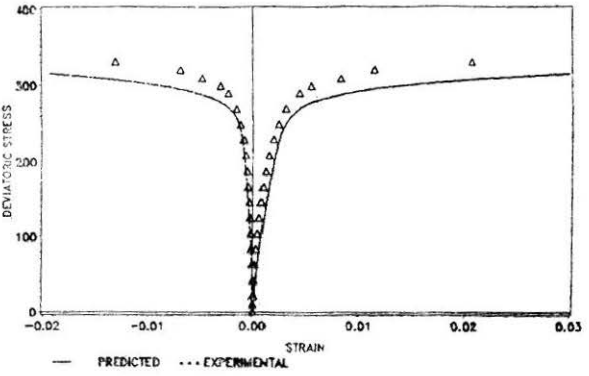

FIGURE 10a Comparison of Stress-Strain Response for Triaxial Compression Test at 30 psi Confining Pressure

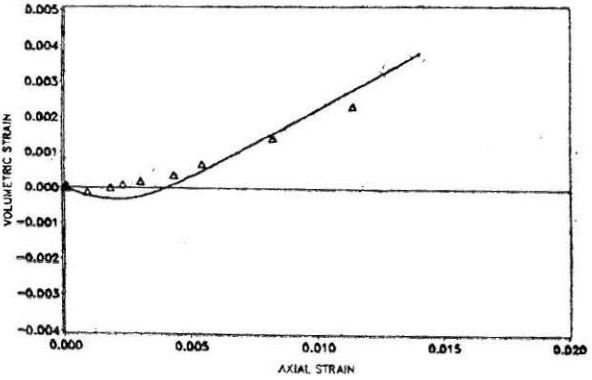

FIGURE 10b Comparison of Volumetric-Axial Strain Response for Triaxial Compression Test at 30 psi Confining Pressure

Comparison of the stress-strain and volumetric-axial strain responses for a *CTC* test at a confining pressure of 104 *Kpa* (15 psi) and a *TC* test at a confining pressure of 207 *Kpa* (30 psi) is presented in Figs. 9 and 10. These tests were not included in the evaluation of material constants. Overall, it is observed that the proposed model is able to predict the onset of dilatancy and subsequent dilatant behavior in an accurate manner. Detailed application of the proposed model is currently in progress and will reported in the subsequent papers.

Conclusions

The concepts of two characteristic states and their representation as characteristic state lines in the stress space are introduced to describe volumetric behavior of cohesionless soil during shearing. The first characteristic state line represents the state of cohesionless soil at failure, while the second characteristic line represents the state at which the rate of volumetric strain momentarily vanishes as the soil passes from the compressive mode of deformation to the dilative mode of deformation during shearing. Explicit forms of the two characteristic state lines in the stress space are proposed and used to develop a constitutive model based on the framework of plasticity theory. The general forms of the characteristic state lines are verified using drained shear test data for a fine sand. Stress-strain and volumetric-axial strain respones are predicted using the proposed model and very good correlations are observed with experimental data

References

ABDULJAUWAD, S.N., FARUQUE, M.O. and AZEEMUDDIN, M. (1989), "Experimental Verification and Numerical Evaluation of the Three-Invariant Department Cap Model for Cohesionless Soil," paper submitted to Computers and Geotechnics.

CHANG, C.S., (1985), "Dilatancy Modelling for Granular Sand in Simple Shear Condition," Proc. 11th Int. Conf. on Soil Mech. and Found. Engrg., San Francisco, pp. 419-422.

DAFALIAS, Y.F. and HARRMANN, L.R., (1982), "Bounding Surface Formulation of Soil Plasticity," Ch. 10, Soil Mechanics—Transient and Cyclic Loads, G.N. Pande and O.C. Zienkiewicz, (Eds.), pp. 253-282.

DE BOER, R., "On Plastic Deformation of Soils," (1988), *Int J. of Plasticity*, Vol. 4, No. 4, pp. 371-391.

DESAI, C.S., (1980), "A General Basis for Yield, Failure and Potential Functions in Plasticity," *Int J. Numer. Anal. Methods Geomech.*, Vol. 4, pp. 361-375.

DESAI, C.S. and FARUQUE, M.O., (1984), "Constitutive Model for (Geological) Materrials," *Journal Engineering Mechanics*, ASCE, Vol. 110, pp. 1391-1408.

DESAI, C.S., SOMASUNDARAM, S. and FRANTZISKONIS, G., (1986), "A Hierarchical Approach for Constitutive Modelling of Geologic Materials," *Int. J. Num. Analyt. Meth. Geomech.*, Vol. 10, No. 3.

DIMAGGIO, F.L. and SANDLER, I.S., (1971), "Material Model for Granular Soils," *J. Eng. Mech. Div.*, ASCE, Vol. 97, No. EM3, pp. 935-950.

DRUCKER, D.C., BIGSON, R.E. and HENKEL, D.J., (1957), "Soil Mechanics and Work Hardening Theories of Plasticity," *Proc. ASCE*, Vol. 122, pp. 338-346.

FARUQUE, M.O. and DESAI, C.S., (1985), "Implementation of a General Constitutive Model for Geological Materials," *Int. J. Num. Analyt. Meth. Geomech.*, Vol. 9, pp. 415-436.

FARUQUE, M.O. and CHANG, C.J., (1986), "New Cap Model for Failure and Yielding of Pressure Sensitive Materials," *J. Eng. Mech. Div.*, ASCE, Vol. 112, No. 10, pp. 1041-1053.

FARUQUE, M.O., (1987), "A Third Invariant Dependent Cap Model for Geological Materials," *Soils and Foundations*, Vol. 27, No. 2, pp. 12-20.

FARUQUE, M.O. and ZAMAN, M.M., (1989), "Characteristic States Experimental Study and Constitutive Modeling of a Beach Sand," Report, School of Civil Engineering, University of Oklahoma.

FUKUSHIMA, S. and TATSUOKA, F., (1984), "Strength and Deformation Characteristics of Saturated Sand at Extremely Low Pressures," *Soils and Foundations*, Vol. 24, No. 4, pp. 30-48.

GHABOUSSI, J. and MOMEM, H., (1982), "Modelling and Analysis of Cyclic Behavior of Sand," Soil Mechanics—Transient and Cyclic Loads, G.N. Pande and O.C. Zienkiewicz, (Eds.), Wiley, Chpt. 12, pp. 313-342.

HARDIN, B.O., (1989), "Low-Stress Dilation Test," *J. Geotech. Eng.*, ASCE, Vol. 115, No. 6, pp. 769-787.

HIRAI, H., (1987), "A Combined Hardening Model for Plasticity for Sands," 2nd Int. Conf. Short Course on Constitutive Laws for Engineering Materials: Theory and Applications, C.S. Desai, et al. (Eds.), Elsevier, pp. 557-564.

HONARMANDEBRAHIMI, A. and ZAMAN, M.M., (1987), "Significance of Testing Procedure and Equipment on Determination of Constitutive Parameters for Soil," Proc. Int. Conf. on Numerical Methods in Eng. : Theory and Applications, held at Swansea, Vol. 2, pp. C18/1-8.

LADE, P.V. and DUNCAN, J.M., (1975), "Elastoplastic Stress-Strain Theory for Cohesionless Soil," *J. Geotech. Eng. Div.*, ASCE, Vol. 101, No. GT10, Oct. pp. 1037-1053.

LADE, P.V., (1977), "Elastic-Plastic Stress-Strain Theory for Cohesionless Soil with Curved Yield Surfaces," *International Journal of Solids and Structures*, Vol. 13, pp. 1019-1035.

LOUNG, M.P., (1980), "Stress-Strain Aspects of Cohesionless Soils under Cyclic and Tranient Loading," Proc. Int. Symposium on Soils under Cyclic and Transient Loading G.N. Pande and O.C. Zienkiewicz (Eds.), Vol. 1, A.A. Balkema, Rotterdam, pp. 315-324.

MROZ, Z., NORRIS, V.A. and ZIENKIEWICZ, O.C., (1978), "An Anisotropic Hardening Model for Soils and Its Application to Cyclic Loading," *Int. J. Numer. Anal. Methods Geomech.*, Vol. 2, pp. 203-221.

MROZ, Z., (1980), "On Hypoelasticity and Plasticity Approaches to Constitutive

Modelling of Inelastic Behavior of Soils," *Int. J. Numer. Anal. Methods Geomech.*, Vol. 4, No. 1, pp. 45-55.

PODGORSKI, J., (1985), "General Failure Criterion for Isotropic Media," *J. Eng. Mech.*, ASCE, 111, 188.

POOROSHASB, H.B. and PIETRUSZEZAK, S., (1985), "On Yielding and Flow of Sand; A Generalized Two Surface Model " *Computer and Geotechnics* Vol. 1 pp. 33-58.

PREVOST, J.H., (1978), "Plasticity Theory for Soil Stress-Strain Behavior," *J. Eng. Mech. Div.*, ASCE, Vol. 104, No. EM-5, Oct. pp. 1177-1194.

SANDLER, I.S., DiMAGGIO, F.L. and BALADI, G.Y., (1976), "Generalized Cap Model for Geological Materials," *J. Geotech. Div.*, ASCE, Vol. 102, No. GT7, pp. 683-699.

VALANIS, K.C. and READ, H.E., (1982), "A New Endochronic Plasticity Model for Soils," Ch. 14, Soil Mechanics—Transient and Cyclic Loads, G.N. Pande and O.C. Zienkiewicz, (Eds.)., pp. 375-468.

ZAMAN, M.M., DESAI, CS. and FARUQUE, M.O., (1982), "An Algorithm for Determining Parameters for Cap Model from Raw Laboratory Test Data," *Proc. 4th Int. Conf. Number Methods Geomech.*, Edmonton, Canada.

ZIENKIEWICZ, O.C. HUMPHESON, C. and LEWIS, R.W., (1975), "Associated and Nonassociated Viscoplasticity and Plasticity in Soil Mechanics," *Geotechnique*, Vol. 25, No. 4, pp. 671-689.

NOMENCLATURE

a	Length of the minor axis of the moving yield surface
A'	Constant used in the function $g(\theta)$
$\bar{A}$	Material constant associated with non-associated formulation
$A(\xi, r_d, \sigma_{ij})$	Measure of plastic modulus
C	Value of J_1 at the intersection of moving cap with the failure surface
C^e_{ijkl}	Elastic constitutive tensor
C^{ep}_{ijkl}	Elasto-plastic constitutive tensor
D	Initial relative density
E	Young's modulus
de^p_{ij}	incremental deviatoric plastic strain tensor
F_c	Compressive yield surface
F_d	Dilating yield surface
G	Shear modulus
$g(\theta)$	A function that accounts for the change in slope of the characteristic state lines with θ
$h_1(D)$, $h_2(D)$	Response functions of initial relative density, D
J_1	First invariant of the stress tensor σ_{ij}
J_{2D}	Second invariant of the deviatoric stress tensor S_{ij}
J_{3D}	Third invariant of the deviatoric stress tensor S_{ij}
K	Bulk modulus
$M(D)$, $N(D)$	Material response functions of initial relative density, D
M_o, N_o	Values of M and N at relative density, $D = 0$, respectively
P_a	Atmospheric pressure
Q_c	Plastic potential function for compressive yield surface
Q_d	Plastic potential function for dilating yield surface
R	Ratio of the major to minor axes of the moving cap
S_{ij}	Deviatoric stress tensor
X	Value of J_1 when moving cap intersects with J_1 axis

α, β, γ	Material constants associated with non-associated formulation
$\beta_1, \beta_2, \eta_1, \eta_2$	Material constants associated with hardening of the material
μ	Material constant associated with the second characteristic state line
ε_{ij}	Strain tensor
ε_{ij}^e	Elastic strain tensor
ε_{ij}^p	Plastic strain tensor
θ	Angle of similarity
λ_1, η_1	Material constants for function $h_1(D)$
λ_2, η_2	Material constants for function $h_2(D)$
V	Poisson's ratio
σ_{ij}	Stress tensor
ξ, ξ_d, r_d	Hardening functions expressed in terms of $d\varepsilon_{ij}^p$ and de_{ij}^p